Creep Crack Growth Properties of Type 308 Austenitic Stainless Steel Weld Metals

The creep crack growth rate of the high-Bi-content flux cored arc weld metal was investigated

BY S. KONOSU, A. HASHIMOTO, H. MASHIBA, M. TAKESHIMA AND T. OHTSUKA

ABSTRACT. Using Type 308 austenitic stainless steel weld metal made by the SMAW and FCAW processes, creep tests and creep crack growth tests were carried out at a temperature of 650°C. Creep crack growth rate tests were conducted using CT-type specimens and the data derived were arranged according to parameter C*. With regard to the flux cored arc weld metal, Bi_2O_3 (melting point 820°C) was intentionally added to the flux for easy slag peeling and enhanced welding operability. The bismuth segregated (segregation depth approximately 15 Å) at the grain boundaries and, due to the presence of this bismuth, fracturing occurred intergranularly, with marked reduction in creep ductility. Further, the creep crack growth rate of the flux cored arc weld metal, which contained large amounts of bismuth, was exceedingly rapid compared with that of SMA and FCA weld metal not containing bismuth. Bismuth that has segregated at the grain boundaries is extremely harmful with respect to creep ductility and creep crack growth properties.

Introduction

Flux cored arc welding (FCAW) is being adopted with increasing frequency with the aim of achieving enhanced efficiency in the welding of austenitic stainless steel pipes for high-temperature service (SUS 304 stainless steel, operating temperature approximately 650–750°C). However, there have been numerous reports (Ref. 1) of cases where intergranular cracking has been found after short-term use of welded joints made by the FCAW process. Some of the reasons for this cracking are believed to be as follows:

1) Hot cracks are caused by internal stresses that develop after solidification and during cooling from an elevated temperature in the welding process.

2) Cracks develop as creep fracture elongation decreases during use.

However, assuming that the aforementioned cracking is ascribable to these causes, as the cracks occur along the grain boundaries, detection of such cracks by nondestructive inspection methods while they are still small is, by their very nature, extremely difficult. Namely, to be able to adequately assess equipment safety in cases where the existence of embedded cracks is assumed, research is necessary with regard to creep crack growth properties that will quantitatively clarify how such cracks will propagate during use of the equipment concerned. Accordingly, the current research has been conducted with the aim of contributing to the assessment of equipment safety by investigating the creep crack growth properties of welded joints made by the shielded metal arc welding (SMAW) and FCAW processes.

S. KONOSU is Associate Professor and A. HASHIMOTO is Graduate Student, Dept. of Mechanical Engineering, Ibaraki University, Ibaraki, Japan. H. MASHIBA is Senior Staff, Reliability Engineer, and M. TAKESHIMA is Manager, Equipment Inspection Section, Marifu Refinery, KOA Oil Co., Ltd., Japan. T. OHTSUKA is Staff, Japan Cooperation Center Petroleum, Tokyo, Japan.

KEY WORDS

Flux Cored Arc Welding
Type 308 Stainless Steel
Creep Properties
Creep Crack Growth Rate
Creep Ductility
Bismuth Addition
Slag Removal
Intergranular Fracture
Bismuth Segregation
Grain Boundary Segregation

Sample Materials

To prepare the welded joints, SUS304H base materials of 22-mm plate thickness (0.05%C, 18.2%Cr, 8.0%Ni) were butt joint welded. The welding process and bismuth content of the weld metal were varied to produce three types of samples. The welded joint sample with a low bismuth content made by the FCAW process was designated Sample NF. The welded joint with a high bismuth content and low C content made by the FCAW process was called Sample NFB and the low bismuth welded joint made by the SMAW process, Sample NS. Sample NS was added to determine whether the difference in welding process due to the noninclusion of Bi would have any influence on creep properties.

Table 1 gives the welding conditions of the NF, NFB and NS materials. DW-308H filler metal with a core diameter of 1.2 mm was used for Sample NF, FCW308LT of 1.2-mm core diameter for Sample NFB and WEL308HTS of 4.0-mm core diameter for Sample NS. Table 2 gives the chemical compositions of the weld metals of the NF, NFB and NS materials. Although all the weld metals are of Type 308 composition, the carbon content of the NF and NS materials exceeds 0.04%, while the carbon content of the NFB material is 0.03%. Furthermore, while the room temperature tensile stress of the welded joints and the minimum specified tensile stress of the base metal for SUS304 at JIS standard are indicated in the table, the tensile stresses of the welded joints exceeded the minimum specified tensile stress of the base metal.

There is no JIS standard for filler metals to weld Type 304H stainless steel, and

Table 1 — Welding Conditions for the NF, NFB and NS Materials

Sample	Welding Procedure	Filler Metal	Shield Gas	Electrode Diameter (mm)	Number of Layers	Current (A)	Voltage (V)	Welding Speed (cm/min)	Interpass Temperature (°C)	Heat Input (J/cm)
NF	FCAW	Type 308	Ar (80%) + CO_2 (20%)	1.2	9	170–200	27–28	20.5–36.8	65–140	9400–15,200
NFB	FCAW	Type 308L	Ar (80%) + CO_2 (20%)	1.2	8	210–220	30–32	25.0–35.3	70–145	11,200–16,100
NS	SMAW	Type 308H	—	4.0	14	140–150	23–25	13.4–19.2	50–140	9600–15,600

Table 2 — Chemical Compositions of the Weld Metals

	C	Si	Mn	P	S	Ni	Cr	Mo	O	N	Bi	δ-ferrite (%) Schaeffler	δ-ferrite (%) DeLong
NF (FCAW)	0.06	0.26	1.33	0.025	0.009	9.44	18.69	0.061	0.034	0.045	< 0.001	3.5	2.8
NFB (FCAW)	0.03	0.65	1.52	0.029	0.003	10.07	20.25	0.038	0.105	0.036	0.023	10.2	11.6
NS (SMAW)	0.059	0.25	1.83	0.013	0.005	9.74	19.6	0.028	0.068	0.03	< 0.001	4.7	5.6

	0.2% Proof Stress (MPa)	Tensile Stress (MPa)
NF (FCAW)	267	691
NFB (FCAW)	264	625
NS (SMAW)	307	583
JIS304 base metal	205 min.	520 min.

Table 3 — Initial Conditions for the Creep Crack Growth Tests

Material	Specimen No.	Initial Crack Length ai/W	Load (kN)
NF	FC-1	0.5	3.06
NFB	FBC-2	0.5	1.96
	FBC-3	0.5	1.47
NS	SC-1	0.5	3.55
	SC-2	0.5	3.06

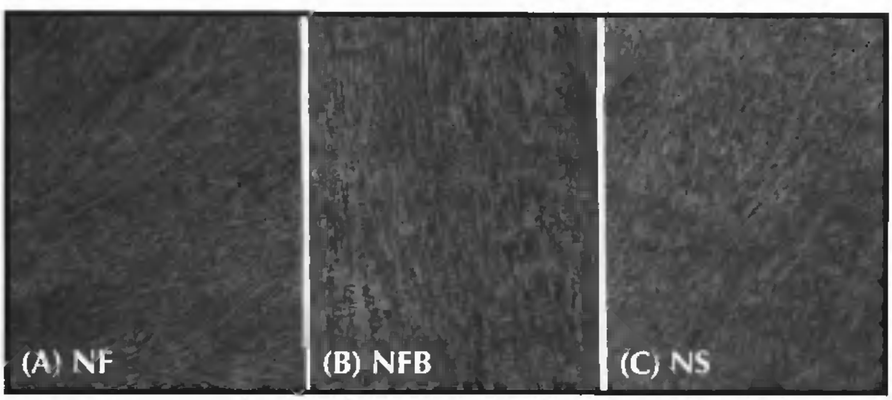

Fig. 1 — Microstructures of the test weld metals at points near the center of thickness (100X).

while AWS has standards for covered electrodes and solid wires to weld stainless steel for high-temperature applications, it has no standards for flux cored wires. Consequently, there have been reports (Ref. 1) of instances where FCAW308L has been used as a filler metal to weld Type 304H steel, as in the case of the NFB material.

According to welding qualification standards (ANSI/AWS D1.1 [Ref. 2], ANSI/ASME B31.3 [Ref. 3] and ASME Sec. IX [Ref. 4]), the requirements for the test results are as follows: 1) The tensile stress at room temperature shall be no less than the minimum of the specified tensile range of the base metal used. 2) The convex surface of the bend specimen shall contain no discontinuities.

Therefore, Type 304 stainless steel welds made by using FCAW308L can be used for elevated temperature service without any problems from the standards aspect, provided they satisfy the foregoing conditions.

While the NFB material contains more than 0.02% bismuth, this is because Bi_2O_3 (melting point 820°C) has been added to the flux intentionally to facilitate slag removal and to enhance welding operability.

Figure 1 shows the microstructures of the weld metals of the NF, NFB and NS materials at points near the center of thickness. While these are all standard dendritic structures, as can be inferred by using the Schaeffler diagram from among the chemical compositions given in Table 2, it was found that the NFB material contained large amounts of delta ferrite.

No evidence whatsoever of solidification cracks was found as a result of observations conducted on the microstructures of the weld metal. In the current study, therefore, it need not be considered that there were any preexisting intergranular microcracks in the test specimens that would contribute to reduced mechanical properties.

As for micro-Vickers Hardness (4.9 N), the hardness of the NFB material, containing the least amount of C, was Hv = 200–220, which was only slightly lower than the hardness of the NF and NS materials (Hv = 200–240).

Experimental Method

Unnotched creep test specimens having a parallel portion of 6.0 mm in diameter and oriented perpendicularly with respect to the weld interface so that the weld metal would be located in the parallel portion, as shown in Fig. 2, were taken from the NF, NFB and NS materials at positions nearest to the upper surface and subjected to creep tests at a test temperature of 650°C. Observations were then made of the fracture surfaces with a scanning electron microscope. Also, a post-test NFB creep specimen was forcibly broken in a vacuum to reveal intergranular fracture surfaces that form within a test piece during creep tests and the elements segregating at the grain boundaries were investigated by carrying out Auger and electron probe microanalyzer (EPMA) analyses.

Additionally, CT-type test specimens with 20% side grooves, as shown in Fig. 3, were taken from weld metals at points near midthickness and subjected to creep crack growth tests at 650°C. A lever-type dead-load test machine was used to perform the tests, of which initial conditions are given in Table 3. Crack length during testing was found by inputting a constant DC current (10 A) from the top and bottom ends of the test specimen, as shown schematically in Fig. 4, measuring the potential drop between points on each side of the crack and converting this to crack length by applying the Johnson's formula given below (Ref. 5). Load line deflection was found by measuring the pull-rod displacement of the test specimen.

$$a = \frac{2W}{\pi} x \cos^{-1}\left[\frac{\cosh(\pi y_0 / 2W)}{\cosh(V / V_0)\left[\cosh^{-1}\left\{\cosh(\pi y_0 / 2W) / \cosh(\pi a_0 / 2W)\right\}\right]}\right] \quad (1)$$

where a = crack length (mm), W = specimen width (mm), a_0 = initial crack length (mm), V_0 = initial voltage (V), y_0 = half distance between the output voltage leads (mm) and V = output voltage (V).

While many fracture mechanics parameters have been suggested for the assessment of creep crack growth properties, the C* parameter defined by substituting the displacement and strain used in the J integral with the displacement rate and strain rate of a material conforming to Norton's law is considered to be suitable as a parameter governing the stress field at the tip of a creep crack (Refs. 6–8).

In the current research, therefore, C* was sought (Refs. 9–11) by means of the following formulas to determine its relationship with creep crack growth rate da/dt (mm/h).

$$C^* = \frac{P\dot{V}_c}{B_N W}\eta\left(\frac{a}{W}\right)$$

$$\eta\left(\frac{a}{W}\right) = \frac{1}{1 - a / W}\frac{n}{n+1}\left(\gamma - \frac{\beta}{n}\right)$$

$$\gamma = \frac{2(1+\alpha)(1 + a / W)(1+\alpha^2) + \alpha(1 - a / W)}{(1 + a / W) + \alpha(1 - a / W)}$$

$$\beta = \frac{\alpha}{\alpha + (1 + a / W)/(1 - a / W)}$$

$$\alpha = \sqrt{\{2a / (W - a)\}^2 + 2\{2a / (W - a)\} + 2} - \{2a / (W - a) + 1\} \quad (2)$$

where, P = load (N), $\dot{V}_C$ = load deflection rate (mm/h), B_N = net thickness of specimen (mm), n = creep exponent in the secondary creep hardening equation.

Results and Discussions

Creep Tests

The results of the creep tests are in Table 4, which gives the relevant applied stress, rupture time, fracture ductility (elongation) and reduction of area, together with the secondary creep rate.

Figure 5 shows the relationship between secondary creep rate and applied stress. For the same value of applied stress, secondary creep rate was fastest for the NFB material, which contained the least carbon, followed by the NS material and NF material, in that order.

The dependence of secondary creep rate on applied stress is expressed by Norton's law as follows:

$$\frac{d\varepsilon}{dt} = k\sigma^n$$

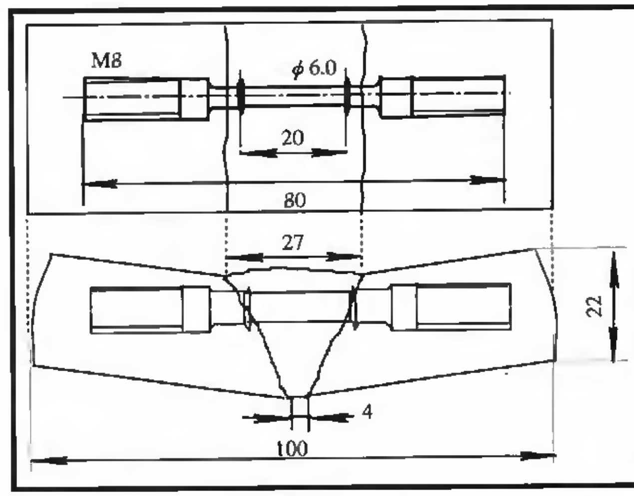

Fig. 2 — Geometry of an unnotched creep specimen and schematic view of specimen orientation.

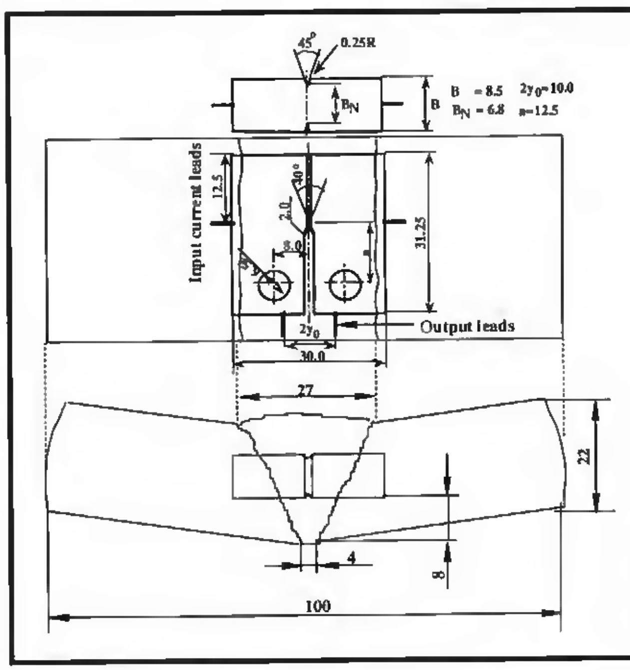

Fig. 3 — Geometry of a compact-type specimen for creep crack growth tests and schematic view of specimen orientation.

Table 4 — Creep Test Results

Sample	Specimen No.	Applied Stress σ (MPa)	Time to Failure tf (h)	Elongation εf (%)	R.A. (%)	Secondary Creep Rate $\dot{\epsilon}$ (h^{-1})
NF	NF-1	156	307.3	20.7	45.3	7.59×10^{-5}
	NF-2	170	42.2	32.2	63.7	1.46×10^{-3}
	NF-3	175	16.6	32.0	68.1	5.50×10^{-3}
	NF-4	145	164.2	33.9	64.0	4.17×10^{-4}
NFB	NFB-1	152	27.1	6.5	11.2	1.17×10^{-3}
	NFB-2	120	152.9	4.5	5.0	7.58×10^{-5}
	NFB-3	110	98.6	1.8	5.3	9.47×10^{-5}
	NFB-4	90	403.7	1.6	3.2	2.52×10^{-6}
	NFB-6	100	219.7	2.0	3.8	8.03×10^{-5}
NS	NS-1	152	183.6	23.1	54.4	2.10×10^{-4}
	NS-3	160	54.5	22.2	60.5	1.06×10^{-3}
	NS-4	140	214.0	24.7	60.0	1.57×10^{-4}

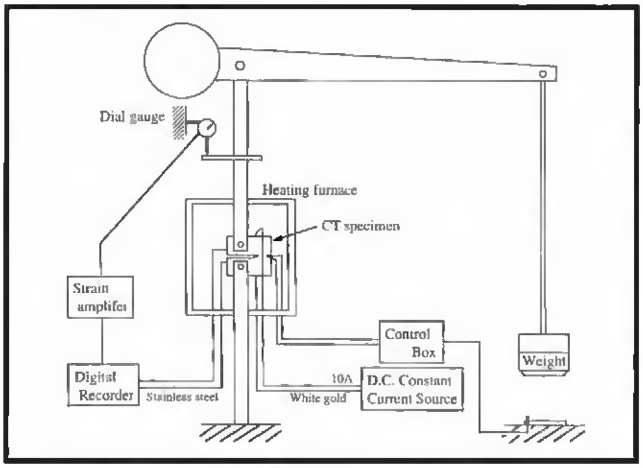

Fig. 4 — Schematic illustration of the creep crack growth test machine.

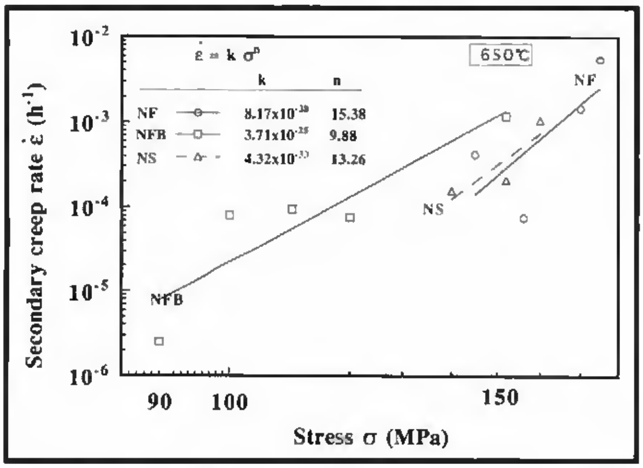

Fig. 5 — Secondary creep rate vs. stress.

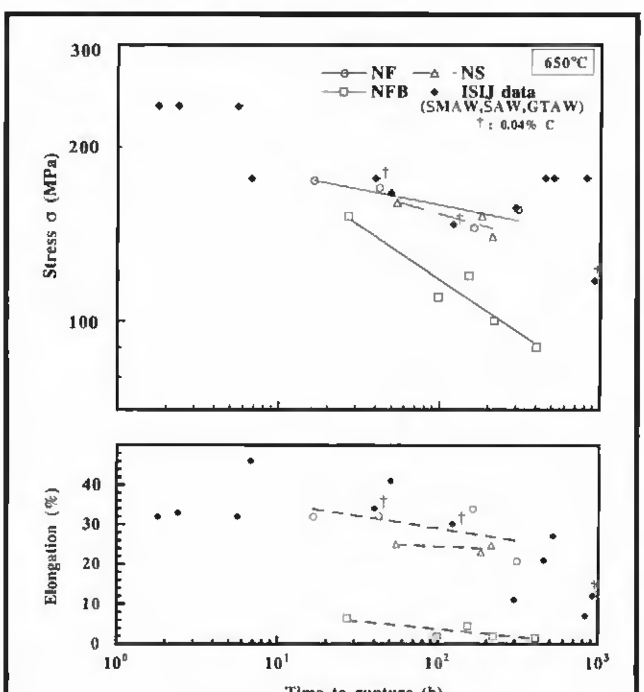

Fig. 6 — Creep rupture properties. (Data with † marks were obtained from specimens with 0.04%C.)

where k and n are constants whose values were obtained from the results of experiments as shown in Fig. 5.

Sample NF : $k = 8.17 \times 10^{-38}$, $n = 15.38$
Sample NFB: $k = 3.71 \times 10^{-25}$, $n = 9.88$
Sample NS : $k = 4.32 \times 10^{-33}$, $n = 13.26$

Figure 6 gives the creep failure properties. Also shown for comparison purposes are the creep failure properties at 650°C of SUS308H stainless steel weld joints made by the shielded metal arc, submerged arc and gas tungsten arc welding processes as given in the *Report on the Mechanical Properties of Metals at Elevated Temperatures*, Vol. V (Ref. 12), put out by The Iron and Steel Institute of Japan (ISIJ). Creep strength and elongation are about the same for both the NS and NF materials, which, furthermore, possess the same properties as those mentioned in ISIJ's published data. On the other hand, creep strength and elongation values were both low for the NFB material.

Namely, while creep ductility was large for the low-Bi-content NS and NF materials regardless of the different welding processes (approximately 25% at creep rupture time of about 100 h), it was extremely low for the high-Bi-content NFB material (approximately 4% at creep rupture time of about 100 h). While the carbon content (0.03%) of the NFB material was lower than that of the other materials, as a reduced carbon content generally causes a decrease in creep-rupture strength and an increase in creep ductility (Ref. 13), it is not considered that the decrease in creep ductility of the NFB material was influenced by carbon content. Furthermore, as the low carbon content (0.04%) weld metal indicated as ISIJ data in the figure has a fracture elongation of about 30% at a rupture time of approximately 100 h, it, too, possesses adequate ductility.

The microscopic structure of a cross section near the fracture surface and SEM fractographs after creep tests are shown in Fig. 7. Unlike the NS and NF materials, cracking in the NFB material propagated mainly along the grain boundaries. Compared with the two other welds, the NFB material contains large amounts of Si and O, as shown in Table 2. Most of the Si and O are believed to be dispersed as fine particles within the grains, in the form of SiO_2 and Bi_2O_3. As a result, grain strength increases and there is a possibility of this being the cause of the decrease in creep ductility of the NFB material. However, the hardness of the NFB material is not great compared to that of the other two welds and its influence, if any, is not considered to be very large.

On the other hand, auger and EPMA analyses were performed on postcreep-test specimens (NFB-6). As a result of conducting EPMA analyses of the fracture surfaces of forcibly induced grain boundary cracking such as that which occurs during creep tests, it was verified that bismuth existed uniformly in the fracture. The results of Auger analyses performed on the grain boundaries are given in Fig. 8. Although bismuth segregation was evident at the grain boundaries of the fracture, as there was no sign of segregation of O, it is believed that bismuth (melting point 270°C) exists as a single substance at the grain boundaries. Figure 9 shows that the distribution of bismuth segregation in the depth direction as determined by argon ion sputtering (30 Å/min) is about 15 Å, indicating that bismuth segregation occurs within an extremely shallow depth at the grain boundaries.

Consequently, it is believed that the sharp drop in creep fracture elongation is due to bismuth segregation at the grain boundaries, as exemplified by the NFB material in Fig. 6.

Therefore, the use of FCAW fluxes containing large amounts of Bi (approximately 0.02%), as in the case of the NFB material, should be avoided with regard to Type 304 stainless welds intended for elevated temperature service.

As the Si contained in large quantities in the NFB material is an element that

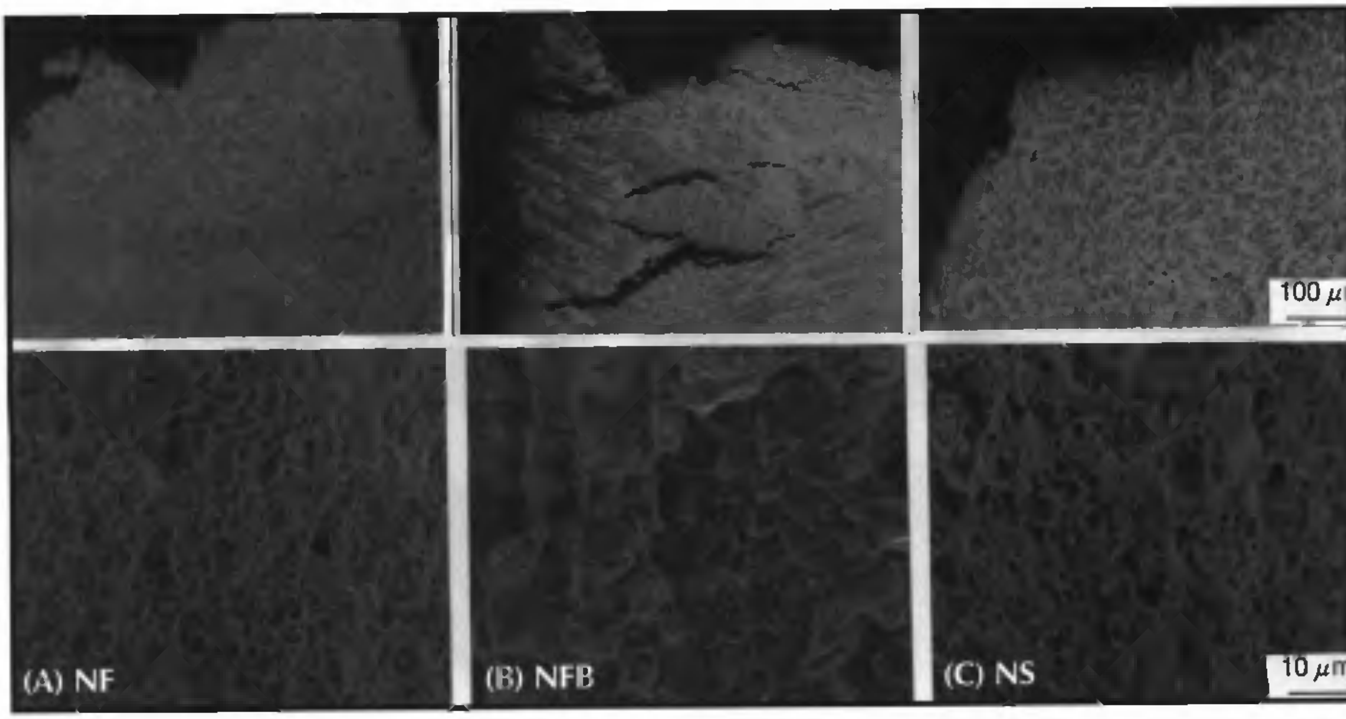

Fig. 7 — Photomicrographs of vicinity of fracture surface and SEM photographs of fracture surface. A — Specimen NF-2 (ε_f = 32.2%); B — specimen NFB-2 (ε_f = 4.5%); C — specimen NS-3 (ε_f = 22.2%).

strongly promotes the ferrite phase, the delta ferrite content of the NFB material is considerably larger than that of the other two welds, as shown in Table 2. Delta ferrite would decompose and produce a sigma phase during high-temperature service. This point should be clarified henceforth as it could constitute the cause of reduced creep ductility.

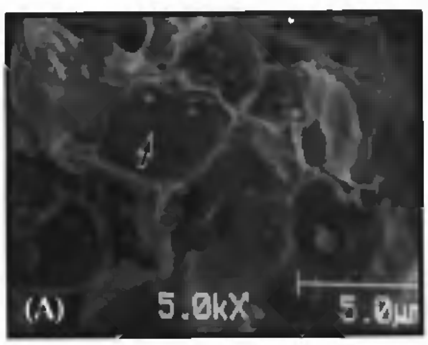

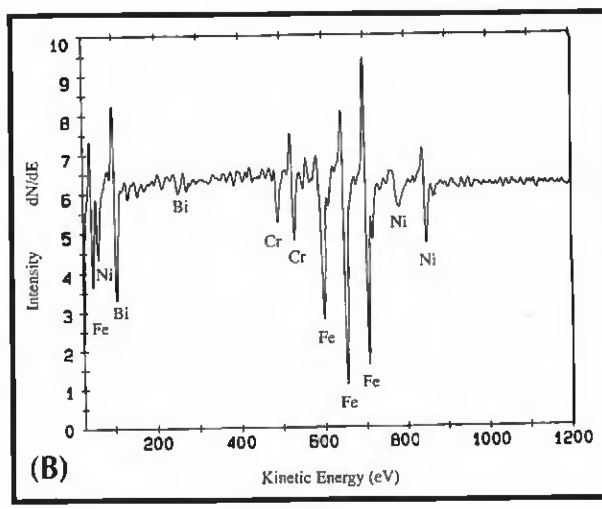

Fig. 8 — Auger spectrum on intergranular fracture surface (creep specimen NFB-6; ε_f = 2.0%).

Creep Crack Growth Test

The relationship between crack length "a" obtained through creep crack growth tests and the changes in load-line deflections, Vc, in relation to time, is shown in Fig. 10A and B. The relationship, derived as a result of the foregoing, between creep crack growth rate (da/dt [mm/h]) and the parameter C* (kJ/m²h) given by Equation 2, is shown in Fig. 11. From this, the following empirical formula was obtained:

$$\frac{da}{dt} = \alpha C^{*\beta}$$

Sample NF :$\alpha = 2.62 \times 10^{-2}$, $\beta = 0.93$
Sample NFB:$\alpha = 5.87 \times 10^{-2}$, $\beta = 0.58$
Sample NS :$\alpha = 8.90 \times 10^{-3}$, $\beta = 1.00$

Comparing the NF, NFB and NS materials in Fig. 11, creep crack growth rate is fastest in the NFB material, which contains large amounts of bismuth, followed by the NF and N5 materials, respectively. Therefore, it is evident that the presence of bismuth that has segregated at the grain boundaries reduces creep ductility and speeds up creep crack growth rate.

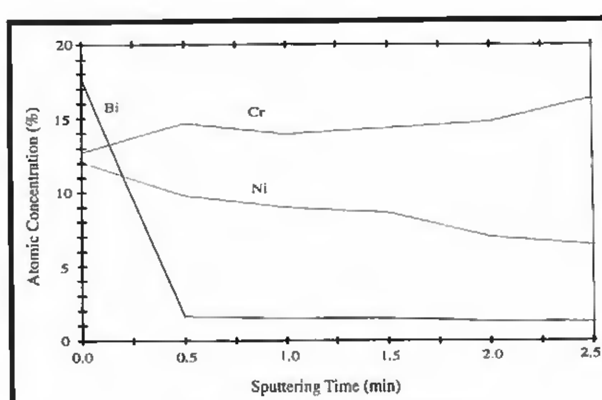

Fig. 9 — Distribution of bismuth in depth direction from intergranular fracture surface.

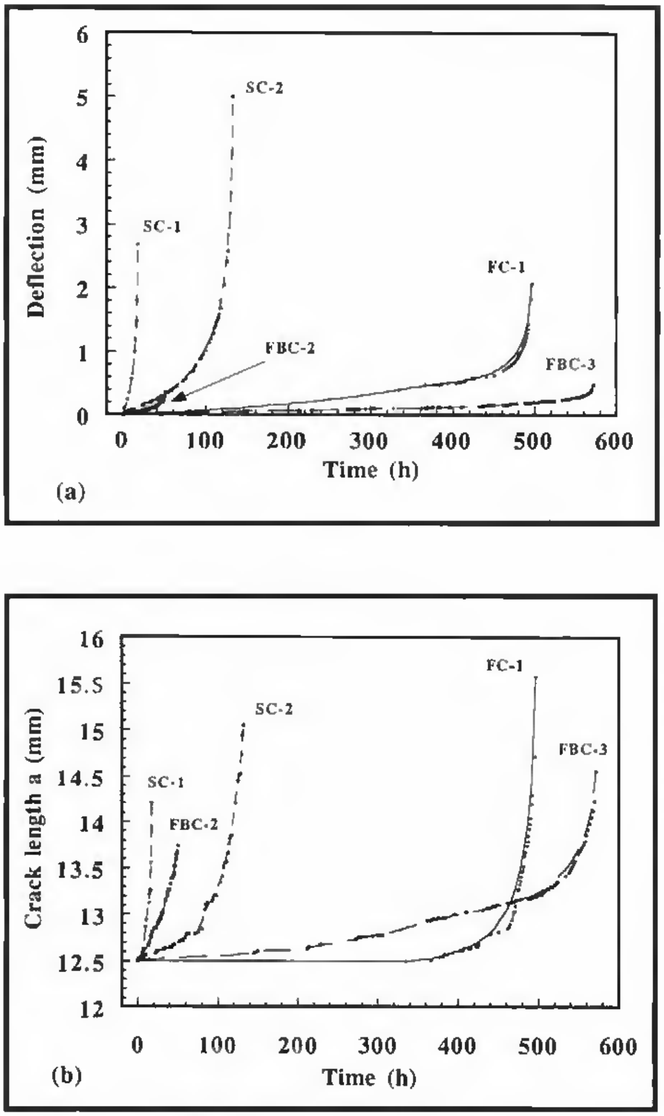

Fig. 10 — A — Creep crack length vs. time; B — load-line deflection vs. time relationship at 650°C.

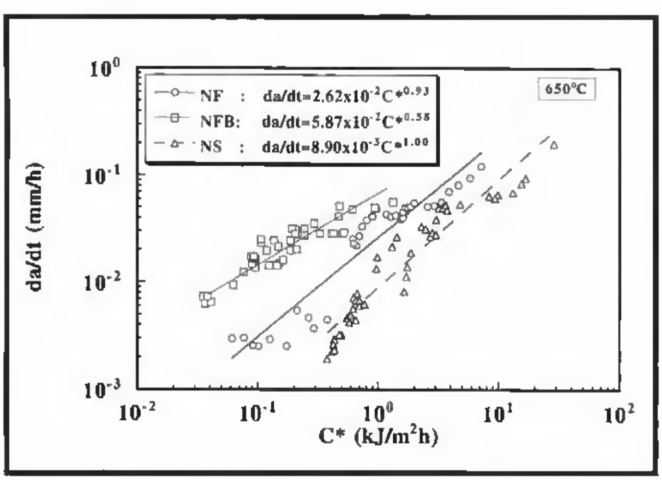

Fig. 11 — Relationship between creep crack growth rate and C parameter at 650°C.*

Conclusions

Using Type 308 austenitic stainless steel weld metal made by the SMAW and FCAW processes, creep tests and creep crack growth tests were conducted at a temperature of 650°C. As a result, the following conclusions were made:

1) In the case of the FCA weld metal (which contained large amounts of bismuth, *i.e.*, >0.02%), bismuth segregated as a single substance at the grain boundaries to a depth of about 15 Å. The presence of this bismuth led to intergranular fracturing and very marked reductions in creep fracture elongation.

2) There was no large difference in creep fracture elongation between the SMA and FCA weld metals, both of which contained no bismuth.

3) Creep crack growth rate of the high-Bi-content FCA weld metal was extremely rapid compared with that of the SMA and FCA weld metals containing no bismuth. In addition to adversely affecting creep elongation properties, the bismuth that segregated at the grain boundaries was also highly deleterious with regard to creep crack growth properties.

4) In view of the foregoing findings, the use of FCAW fluxes containing large amounts of Bi (approximately 0.02%) should be avoided in connection with Type 304 stainless steel welds intended for elevated temperature service.

References

1. Chemical Plant Welding Research Committee of the Japan Welding Engineering Society (JWES). 1996. High temperature damage to stainless steel welds made by flux cored arc welding and its analysis. API 61st Fall Refinery Meeting Oct.: 21–23.

2. ANSI/AWS D1.1, *Structural Welding Code — Steel*. 1986. Section 5.12, Test Results Required. American Welding Society, Miami, Fla.

3. ANSI/ASME B31.3, *Chemical Plant and Petroleum Refinery Piping*. 1984. Section 327.5, Qualification for Welding.

4. ASME *Boiler and Pressure Vessel Code*. 1995. Sec. IX, Qualification Standard for Welding and Brazing Procedures, Welders, Brazers and Welding and Brazing Operators, QW-150 Acceptance Criteria.

5. Johnson, H. H. 1965. *Materials Research and Standards*, 5(9): 442–445.

6. Landes, J. D., and Begley, J. A. 1976. *Mechanics of Crack Growth*, ASTM STP 590, American Society for Testing and Materials, Philadelphia, Pa.: 128–148.

7. Nikbin, K. M., Webster, G. A., and Turner, C. E. 1976. *Cracks and Fracture*, ASTM STP 601, American Society for Testing and Materials, Philadelphia, Pa.: 47–62.

8. Ohji, K., Ogura, K., and Kubo, S. 1976. *Transactions of the Japan Society of Mechanical Engineers*, 42(354): 350–358.

9. Saxena, A. 1976. *Fracture Mechanics: Twelfth Conference*, ASTM STP 700, American Society for Testing and Materials, Philadelphia, Pa.: 131–151.

10. Ernst, M. A. 1983. *Fracture Mechanics: Fourteenth Symposium*, Vol. I, Theory and Analysis, ASTM STP 791, American Society for Testing and Materials, Philadelphia, Pa.: I-499 to I-599.

11. Konosu, S., and Maeda, K. 1989. *Creep Embrittlement Susceptibility and Creep Crack Growth Behavior in Low-Alloy Steels*, ASTM STP 995, American Society for Testing and Materials, Philadelphia, Pa.: 127–152.

12. The Iron and Steel Institute of Japan. 1985. *Report on the Mechanical Properties of Metals at Elevated Temperatures*. Vol. V, Deposited metals, weld metal and welded joints, 38: 185–197.

13. Swindeman, R. W., Sikka, V. K., and Klueh, R. L. 1983. Residual and trace element effects on the high-temperature creep strength of austenitic stainless steel. *Metallurgical Transactions*, 14A.: 581–593.